

Testing an Approximation to Large- N_c QCD with a Toy Model

Maarten Golterman^a, Santiago Peris^b, Boris Phily^c and Eduardo de Rafael^c

^a Institute for Nuclear Theory, University of Washington
Box 351550, Seattle, WA 98195, USA, and
Dept. of Physics and Astronomy, San Francisco State University
1600 Holloway Ave, San Francisco, CA 94132, USA

^b Grup de Física Teòrica and IFAE
Universitat Autònoma de Barcelona, 08193 Barcelona, Spain

^c Centre de Physique Théorique
CNRS-Luminy, Case 907
F-13288 Marseille Cedex 9, France

Abstract

We consider a simple model of large- N_c QCD defined by a spectrum consisting of an infinite set of equally spaced zero-width vector resonances. This model is an excellent theoretical laboratory for investigating certain approximation schemes which have been used recently in calculations of hadronic parameters, such as the Minimal Hadronic Approximation. We also comment on some of the questions concerning issues of *local duality* versus *global duality* and finite-energy sum rules.

1 Introduction

The suggestion to keep the number of colours N_c in QCD as a free parameter was made by 't Hooft [1] as a possible way to approach the study of non-perturbative phenomena. In spite of the efforts of many illustrious theorists who have worked on the subject, QCD in the large- N_c limit still remains unsolved. However, many interesting properties have been proved¹ which suggest that, indeed, the theory in this limit has the bulk of the non-perturbative properties of three-colour QCD. In particular, it has been shown that, if confinement persists in this limit, there is spontaneous chiral symmetry breaking [4].

The spectrum of the theory in the large- N_c limit consists of an infinite number of narrow stable meson states which are flavour nonets [5]. This spectrum, however, looks *a priori* not quite like the one in the real world. The vector and axial-vector spectral functions measured in $e^+e^- \rightarrow$ hadrons and in hadronic τ decay show indeed a richer structure than just a sum of narrow states. There are, however, many instances where one is only interested in observables which are given by weighted integrals of hadronic spectral functions. In these cases, it may be enough to know a few *global* properties of the hadronic spectrum in order to have a good interpolation. Typical examples of that are the coupling constants of the effective chiral Lagrangian of QCD at low energies, as well as the coupling constants of the effective chiral Lagrangian of the electroweak interactions of pseudo-scalar particles in the Standard Model. It has been shown in some examples [6, 7, 8, 9, 10] that inserting the hadronic spectrum of large- N_c QCD as an approximation to the real hadronic spectrum provides rather good results. It is in this sense that large- N_c QCD seems to be a very useful phenomenological approach for understanding non-perturbative QCD physics at low energies.

In most cases of interest, the Green's functions which govern the low-energy constants of the chiral Lagrangian are two-point functions with zero-momentum insertions of vector, axial-vector, scalar and pseudo-scalar currents. The higher the power in the chiral expansion, the higher the number of insertions. Furthermore, they are order parameters of spontaneous chiral symmetry breaking; i.e. they vanish, in the chiral limit where the light quark masses are set to zero, order by order in the perturbative vacuum of QCD. That implies that they have a power-like fall-off in $1/Q^2$ at large Q^2 ; where $Q^2 = -q^2 \geq 0$ in the euclidean region, with q the four-momentum flowing through the Green's function. When $N_c \rightarrow \infty$, within a finite radius in the complex Q^2 plane centered at the origin, these Green's functions only have a *finite number of poles*. The restriction to the minimal number of poles required to satisfy the known *short-distance* and *long-distance* QCD constraints results in a simple approximation which we call the *minimal hadronic approximation* (MHA) to large- N_c QCD. In the cases which we have been able to test, this minimal approximation gives already very good phenomenological results. The MHA is in principle improvable: considering more terms in the OPE of the two currents in the underlying Green's function through which the q -momentum flows provides extra algebraic sum rules which can be used to fix the extra hadronic parameters. Also, knowing more terms at small- Q^2 values, in the chiral expansion of the same underlying Green's function, provides extra algebraic sum rules of a similar nature. Unfortunately, in most cases of interest, it is difficult to carry on these improvements in practice, and the nature of the MHA in real QCD remains unclear. This is the reason to resort to *simple models*, where the full large- N_c -like spectrum is fixed *a priori* and one can study approximations and their improvements explicitly. In this paper we shall study a model defined by a spectrum of an infinity of zero-width vector particles whose masses (squared) are equally spaced. We consider this spectrum quite realistic. As a matter of fact, for large masses, this *is* the spectrum of QCD at large N_c in 2 dimensions (where the theory can be solved [11]) and, in the case of our four-dimensional world, this is also the spectrum of the daughter trajectories of Regge Theory; which has long been suspected to be a good effective description of QCD in the large- N_c limit.

To the best of our knowledge, this type of model was first proposed in the context of QCD in ref. [12]. More recent studies confronting phenomenology can be found in ref. [13, 14]. Also recently Shifman [15] has emphasized the usefulness of this model for investigating the question of *local duality* versus *global duality*. The model has very intriguing connections with functions which appear profusely in analytic number theory.

¹For recent reviews, see e.g. the book in ref. [2] and the lectures in ref. [3].

The paper is organized as follows. In section 2, we introduce the model with equally spaced, infinitely narrow resonances. We then take the vector-current two-point function (more precisely, the Adler function) as a laboratory, and calculate it in this model, including its OPE and chiral expansions. In section 3 we consider a specific form of the minimal hadronic approximation. After some discussion of its nature, we give explicit numerical examples of how the MHA approximates the Adler function of our model. Finally, in section 4, we compare the hadronic branching ratio for τ decay between the model, the OPE and the MHA, in order to see how the MHA performs with respect to local duality and finite-energy sum rules.

2 The model

Let us consider the vector–vector correlator defined by

$$i \int d^4x e^{iq \cdot x} \langle 0 | T (J^\mu(x), J^\nu(0)) | 0 \rangle = (q^\mu q^\nu - g^{\mu\nu} q^2) \Pi(Q^2 \equiv -q^2), \quad (2.1)$$

with J^μ the electromagnetic current of light quarks, for example. The model for this correlator consists of an infinite number of equally spaced narrow states as illustrated in Fig. 1 below. With M_0 the mass of the lowest state and σ the spacing mass, the spectrum is given by

$$\frac{1}{\pi} \text{Im} \Pi(t) = A \sigma^2 \sum_{n=0}^{\infty} \delta(t - M_0^2 - n\sigma^2), \quad (2.2)$$

with A an arbitrary normalization factor that will be determined below.

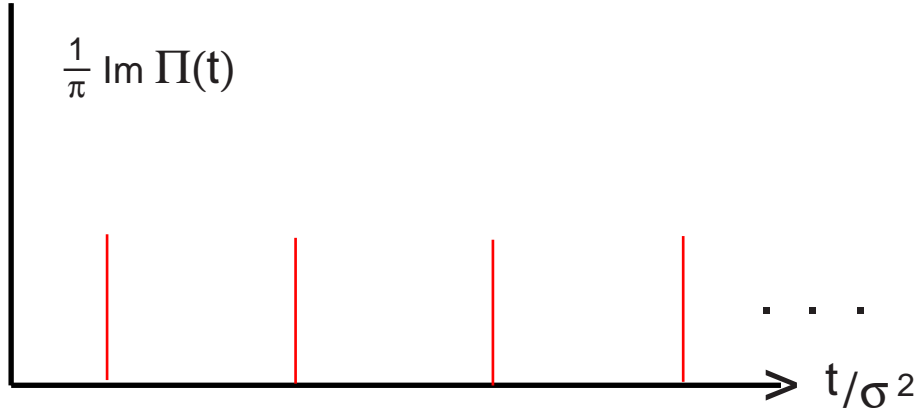


Fig. 1 The vector spectral function in the toy model of large- N_c QCD.

Of special interest for our discussion is the Adler function defined as follows:

$$A(Q^2) = -Q^2 \frac{d}{dQ^2} \Pi(Q^2) = \int_0^\infty dt \frac{Q^2}{(Q^2 + t)^2} \frac{1}{\pi} \text{Im} \Pi(t) \quad (2.3)$$

$$= A \frac{Q^2}{\sigma^2} \sum_{n=0}^{\infty} \frac{1}{\left(\frac{Q^2}{\sigma^2} + \frac{M_0^2}{\sigma^2} + n\right)^2} \equiv A \frac{Q^2}{\sigma^2} \zeta\left(2, \frac{Q^2 + M_0^2}{\sigma^2}\right), \quad (2.4)$$

where $\zeta\left(2, \frac{Q^2+M_0^2}{\sigma^2}\right)$ is the so-called *generalized Riemann zeta function* [16], sometimes called the *Hurwitz function*². We can choose the normalization factor A so that the large- Q^2 behaviour of the Adler function reproduces the parton like *asymptotic freedom* behaviour predicted by perturbative QCD. This can be readily seen using the Euler–Maclaurin formula:

$$\frac{1}{\left(\frac{Q^2}{\sigma^2} + \frac{M_0^2}{\sigma^2}\right)^2} + \frac{1}{\left(\frac{Q^2}{\sigma^2} + \frac{M_0^2}{\sigma^2} + 1\right)^2} + \dots + \frac{1}{\left(\frac{Q^2}{\sigma^2} + \frac{M_0^2}{\sigma^2} + N\right)^2} = \quad (2.5)$$

$$\int_0^N dx \frac{1}{\left(\frac{Q^2}{\sigma^2} + \frac{M_0^2}{\sigma^2} + x\right)^2} + \frac{1}{2} \left[\frac{1}{\left(\frac{Q^2}{\sigma^2} + \frac{M_0^2}{\sigma^2}\right)^2} + \frac{1}{\left(\frac{Q^2}{\sigma^2} + \frac{M_0^2}{\sigma^2} + N\right)^2} \right] + \dots, \quad (2.6)$$

and the integral result

$$\int_0^N dx \frac{1}{\left(\frac{Q^2}{\sigma^2} + \frac{M_0^2}{\sigma^2} + x\right)^2} = \frac{-1}{\frac{Q^2}{\sigma^2} + \frac{M_0^2}{\sigma^2} + N} - \frac{-1}{\frac{Q^2}{\sigma^2} + \frac{M_0^2}{\sigma^2}}. \quad (2.7)$$

Letting $N \rightarrow \infty$ we get the result

$$\lim_{Q^2 \rightarrow \infty} \mathcal{A}(Q^2) \Rightarrow A, \quad (2.8)$$

which, for $A = \frac{N_c}{16\pi^2} \frac{4}{3}$, reproduces the asymptotic parton limit result. For simplicity, we shall take $A = 1$ from here onwards.

There is an integral representation of the Hurwitz function which will be very useful for our purposes:

$$\zeta(s, z) = \frac{1}{\Gamma(s)} \int_0^\infty dt e^{-zt} \frac{t^{s-1}}{1 - e^{-t}} \quad (\text{Re } s > 1 \quad \text{and} \quad \text{Re } z > 0). \quad (2.9)$$

2.1 OPERATOR PRODUCT EXPANSION OF THE MODEL

In QCD, the behaviour of the Adler function in the physical vacuum, for large euclidean Q^2 values, can be obtained from the operator product expansion (OPE) of the two currents in Eq. (2.1) and it results in an expansion in $1/Q^2$ powers à la Shifman, Vainshtein, Zakharov [17]. In the model this expansion follows readily from the integral representation (2.9) applied to $\zeta\left(2, \frac{Q^2+M_0^2}{\sigma^2}\right)$.

Using the fact that

$$e^{xz} \frac{z}{e^z - 1} = \sum_{n=0}^{\infty} B_n(x) \frac{1}{n!} z^n, \quad (2.10)$$

is the generating function of the Bernoulli polynomials,³ we have

$$e^{-\frac{M_0^2}{\sigma^2}t} \frac{t}{1 - e^{-t}} = e^{\left(1 - \frac{M_0^2}{\sigma^2}\right)t} \frac{t}{e^t - 1} = \sum_{n=0}^{\infty} B_n\left(1 - \frac{M_0^2}{\sigma^2}\right) \frac{1}{n!} t^n, \quad (2.11)$$

and using the symmetry property in Eq. (A.13), plus the Laplace transform integral representation

$$\frac{1}{s^{n+1}} = \frac{1}{\Gamma(n+1)} \int_0^\infty dt e^{-st} t^n, \quad (2.12)$$

we get the required OPE-like expansion

²It also coincides with $\psi'\left(\frac{Q^2+M_0^2}{\sigma^2}\right)$, where $\psi'(z) = \frac{d^2}{dz^2} \log \Gamma(z)$ and $\Gamma(z)$ is Euler's Gamma function.

³For the sake of completeness we list a few useful properties of the Bernoulli polynomials in an Appendix.

$$\mathcal{A}^{(\infty)}(Q^2) = \sum_{n=0}^{\infty} (-1)^n B_n(\hat{M}_0^2) \left(\frac{\sigma^2}{Q^2} \right)^n, \quad \text{with} \quad \hat{M}_0^2 \equiv \frac{M_0^2}{\sigma^2}. \quad (2.13)$$

The explicit expansion for the first few terms is then

$$\begin{aligned} \mathcal{A}^{(\infty)}(Q^2) \rightarrow & 1 + \left(\frac{1}{2} - \hat{M}_0^2 \right) \left(\frac{\sigma^2}{Q^2} \right) + \left(\frac{1}{6} - \hat{M}_0^2 + \hat{M}_0^4 \right) \left(\frac{\sigma^2}{Q^2} \right)^2 \\ & + \left(-\frac{\hat{M}_0^2}{2} + \frac{3\hat{M}_0^4}{2} - \hat{M}_0^6 \right) \left(\frac{\sigma^2}{Q^2} \right)^3 + \left(-\frac{1}{30} + \hat{M}_0^4 - 2\hat{M}_0^6 + \hat{M}_0^8 \right) \left(\frac{\sigma^2}{Q^2} \right)^4 + \mathcal{O} \left(\frac{\sigma^2}{Q^2} \right)^5. \end{aligned} \quad (2.14)$$

In QCD, and in the chiral limit where the light quark masses are set to zero, there is no $1/Q^2$ term in the OPE, because there is no local operator of dimension $d = 2$. We can then make the model look like QCD more closely by imposing this property in Eq. (2.14) as well, which requires that

$$M_0^2 = \frac{1}{2} \sigma^2. \quad (2.15)$$

The model has then only one mass scale σ^2 ; furthermore, because of the property of the Bernoulli polynomial that

$$B_{2n+1}(1/2) = 0, \quad \text{for} \quad n \geq 0, \quad (2.16)$$

the equivalent of the OPE of the Adler function in the model, has only *even* $1/Q^2$ powers:

$$\mathcal{A}^{(\infty)}(Q^2) \rightarrow 1 - \frac{1}{12} \left(\frac{\sigma^2}{Q^2} \right)^2 + \frac{7}{240} \left(\frac{\sigma^2}{Q^2} \right)^4 - \frac{31}{1344} \left(\frac{\sigma^2}{Q^2} \right)^6 + \dots, \quad (2.17)$$

and the vacuum expectation values appearing in the OPE are then given by the values of the Bernoulli polynomials at $x = 1/2$. For the rest of the paper we shall keep $M_0^2 = \sigma^2/2$ and comment on the relevance of this constraint whenever necessary.

It is easy to see that the OPE series of the model in question is a divergent series. From Eq. (A.15) it follows that

$$B_{2N}(1/2) = (-1)^{N+1} 2(2N)! \frac{1}{(2\pi)^{2N}} \sum_{n=1}^{\infty} \frac{(-1)^n}{n^{2N}}, \quad (2.18)$$

and the sum of the series on the right-hand side is known:

$$\sum_{n=1}^{\infty} \frac{(-1)^n}{n^{2N}} = \frac{(1 - 2^{2N-1}) \pi^{2N}}{(2N)!} |B_{2N}|, \quad (2.19)$$

which results in

$$B_{2N}(1/2) = (-1)^N \left(1 - \frac{1}{2^{2N-1}} \right) |B_{2N}|, \quad N > 0. \quad (2.20)$$

From this, it is easy to see that the series is divergent because

$$\lim_{N \rightarrow \infty} \frac{|B_{2N}(1/2)| \left(\frac{\sigma^2}{Q^2} \right)^{2N}}{|B_{2N-2}(1/2)| \left(\frac{\sigma^2}{Q^2} \right)^{2N-2}} = \lim_{N \rightarrow \infty} \frac{|B_{2N}|}{|B_{2N-2}|} \left(\frac{\sigma^2}{Q^2} \right)^2 \sim \left(\frac{N}{\pi} \frac{\sigma^2}{Q^2} \right)^2, \quad (2.21)$$

where we have used the property that asymptotically,

$$\lim_{N \rightarrow \infty} |B_{2N}| \sim 4\sqrt{\pi} \frac{N^{2N+1/2}}{(e\pi)^{2N}}. \quad (2.22)$$

At orders

$$2N \gtrsim 2\pi \frac{Q^2}{\sigma^2}, \quad (2.23)$$

the OPE ceases to be an improving expansion.

The OPE series is divergent, but summable. In fact, the Borel sum of the OPE series is precisely the Adler function defined by the generalized Riemann zeta function. To see this, recall that the Borel sum of the series in Eq. (2.13) is defined as follows

$$\sum_{n=0}^{\infty} (-1)^n B_n(1/2) \left(\frac{\sigma^2}{Q^2} \right)^n \rightarrow \int_0^{\infty} dt e^{-t} \sum_{n=0}^{\infty} (-1)^n \frac{B_n(1/2)}{n!} \left(\frac{\sigma^2}{Q^2} t \right)^n. \quad (2.24)$$

If now, we use again the symmetry property in Eq. (A.13) and the second of Eq. (2.11); plus the change of variables $\tilde{t} = t \frac{\sigma^2}{Q^2}$, one obtains the desired result.

2.2 CHIRAL PERTURBATION THEORY EXPANSION OF THE MODEL

We can also find, in this model, the equivalent of the chiral perturbation theory (χ PT) expansion of the Adler function; i.e., the Taylor expansion at small Q^2 values. For that, it is sufficient to expand the term $e^{-\frac{Q^2}{\sigma^2}t}$ in the integral representation of Eq. (2.9) with the result

$$\mathcal{A}^{(0)}(Q^2) = \sum_{n=0}^{\infty} (-1)^n \left(\frac{Q^2}{\sigma^2} \right)^{n+1} (n+1) \zeta \left(n+2, \frac{M_0^2}{\sigma^2} \right). \quad (2.25)$$

With $M_0^2 = \frac{1}{2}\sigma^2$, and using the property that

$$\zeta(s, 1/2) = (2^s - 1) \zeta(s), \quad \text{for } s > 1, \quad (2.26)$$

the series becomes

$$\mathcal{A}^{(0)}(Q^2) = \sum_{n=0}^{\infty} (-1)^n (n+1) \left[2^{(n+2)} - 1 \right] \zeta(n+2) \left(\frac{Q^2}{\sigma^2} \right)^{n+1}, \quad (2.27)$$

i.e., the low-energy constants of the Adler function are proportional to Riemann's zeta functions of increasing argument. The explicit chiral expansion for the first few terms gives

$$\mathcal{A}^{(0)}(Q^2) \rightarrow \frac{\pi^2}{2} \left(\frac{Q^2}{\sigma^2} \right) - 14 \zeta(3) \left(\frac{Q^2}{\sigma^2} \right)^2 + \frac{\pi^4}{2} \left(\frac{Q^2}{\sigma^2} \right)^3 - 124 \zeta(5) \left(\frac{Q^2}{\sigma^2} \right)^4 + \mathcal{O} \left(\frac{Q^2}{\sigma^2} \right)^5. \quad (2.28)$$

Numerically,

$$\mathcal{A}^{(0)}(Q^2) \rightarrow 4.9348 \left(\frac{Q^2}{\sigma^2} \right) - 16.8288 \left(\frac{Q^2}{\sigma^2} \right)^2 + 48.7045 \left(\frac{Q^2}{\sigma^2} \right)^3 - 128.579 \left(\frac{Q^2}{\sigma^2} \right)^4 + \dots. \quad (2.29)$$

The chiral expansion is convergent within a radius $\frac{Q^2}{\sigma^2} \leq \frac{1}{2}$.

It is indeed amusing that a model of a well defined limit of a rather complicated quantum field theory like QCD, has such direct connections with the basic functions of analytic number theory and transcendental numbers.

3 The Minimal Hadronic Approximation.

We want to study how good is the approximation which consists in replacing the exact spectral function in Eq. (2.2) by a finite set of low states, say $m+1$, with arbitrary masses \tilde{M}_n^2 , and lumping the rest into the equivalent of a perturbative QCD continuum starting at a mass squared value s_0 :

$$\frac{1}{\pi} \text{Im} \Pi(t) \Big|_{\text{MHA}}^{(m+1)} = \sigma^2 \sum_{n=0}^m \delta(t - \tilde{M}_n^2) + \theta(t - s_0). \quad (3.30)$$

The approximated spectrum is illustrated in Fig. 2. We call this the *minimal hadronic approximation* (MHA), by analogy to the approximations which we have been making in real large- N_c QCD.⁴

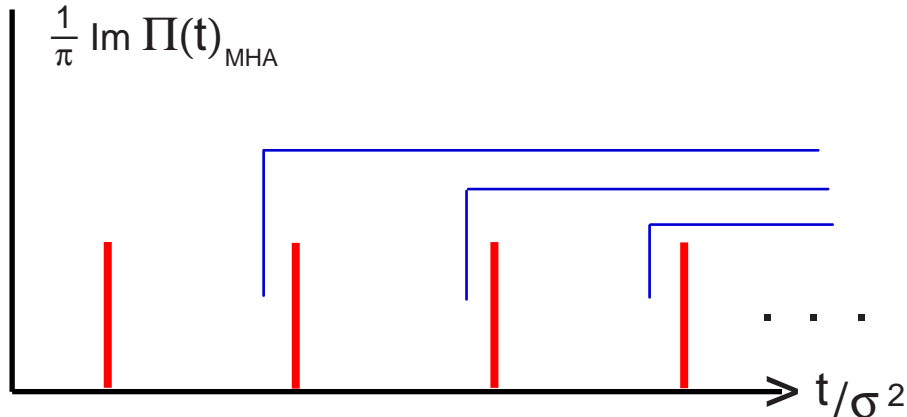


Fig. 2 The Minimal Hadronic Approximation (MHA) to the vector spectral function in the toy model of large- N_c QCD. The successive approximations correspond to one state plus continuum (the first blue band), two states plus continuum (the second blue band), three states plus continuum, etc.

The MHA spectrum leads to the following form for the Adler function:

$$\mathcal{A}(Q^2)|_{\text{MHA}}^{(m+1)} = \frac{Q^2}{\sigma^2} \sum_{n=0}^m \frac{1}{\left(\frac{Q^2}{\sigma^2} + \frac{\tilde{M}_n^2}{\sigma^2}\right)^2} + \frac{Q^2}{Q^2 + s_0}, \quad (3.31)$$

where the second term is the one induced by the perturbative continuum. The OPE-like expansion of the MHA approximation to the toy model can be easily obtained from the expression above, with the result

$$\mathcal{A}^{(\infty)}(Q^2)|_{\text{MHA}} = 1 + \sum_{N=1}^{\infty} (-1)^N \left[\left(\frac{s_0}{\sigma^2}\right)^N - N \sum_{n=0}^m \left(\frac{\tilde{M}_n^2}{\sigma^2}\right)^{N-1} \right] \left(\frac{\sigma^2}{Q^2}\right)^N. \quad (3.32)$$

We fix the onset of the continuum s_0 to match the leading $1/Q^2$ term of the OPE for the Adler function, which vanishes. This results in the condition⁵

$$s_0 = (m+1)\sigma^2. \quad (3.33)$$

The masses \tilde{M}_N^2 of the explicit narrow states are then fixed so as to satisfy more and more constraints provided by the OPE and the χ PTE expansions of the underlying theory. This results in a system of equations:

$$(m+1)^N - N \sum_{n=0}^m \left(\frac{\tilde{M}_n^2}{\sigma^2}\right)^{N-1} = B_N(1/2), \quad \text{for } N = 2, 3, \dots, \quad (3.34)$$

⁴See ref. [18] for a recent review, and refs. [6] to [10] for details.

⁵If $\tilde{M}_0^2 \neq 1/2$, Eq. (3.33) reads $s_0 = \sigma^2(m+1/2 + \tilde{M}_0^2)$. Notice that s_0 should always be larger than the mass of the last resonance kept explicitly in the spectrum.

from the OPE constraints; and another system of equations

$$\begin{aligned} \frac{1}{N(m+1)^N} + \sum_{n=0}^m \left(\frac{\sigma^2}{\tilde{M}_n^2} \right)^{N+1} &= \zeta\left(N+1, \frac{1}{2}\right) \\ &= \sum_{n=0}^{\infty} \frac{1}{\left(n + \frac{1}{2}\right)^{N+1}}, \quad \text{for } N = 1, \dots, \end{aligned} \quad (3.35)$$

from the χ PT constraints. The idea is to solve these equations for successive values of the number m of explicit narrow states. Looking at Eq. (3.35) one sees that the first term on the left-hand side vanishes in the $m \rightarrow \infty$ limit. It is clear that, in this limit, the system of equations (3.35) has as a solution $\tilde{M}_n^2 = \sigma^2(n + 1/2)$, i.e. the true spectrum.

We also find (numerically, including up to nine resonances) that when one substitutes the masses found from only the χ PT constraints into the left-hand side of eq. (3.34), the resulting numbers converge to the values given by the right-hand side (i.e. the $B_N(1/2)$). This implies that in principle, the MHA will converge to the exact result for *all* values of Q^2 , even if one uses *only* small Q^2 information. However, the convergence is rather slow for large Q^2 . Therefore, in practice, one would expect better convergence if one also uses constraints coming from the OPE in determining the parameters \tilde{M}_n^2 of the MHA.

It is less clear what the nature is of the system of equations following from using only OPE constraints since, unlike the χ PT expansion, the OPE is an asymptotic expansion (see section (2.1)). For a given number of OPE constraints, $2N$, Eq. (2.23) gives a value of Q^2 below which the MHA obtained by solving the set of equations (3.34) may be wrong.⁶ Conversely, given a value of Q^2 above which one wishes to obtain a good approximation to the exact model, eq. (2.23) gives an estimate of the maximum useful order of the OPE. However, as already alluded to above, we find it quite plausible to expect that using a few constraints coming from the OPE in addition to those from χ PT should speed up the convergence in the region of *large* Q^2 , relative to a MHA solely based on χ PT constraints. In practice, quantities which typically one encounters in QCD correspond to integrals of the Adler function weighted by a known function, and inspection of the weight function should dictate the optimal choice of short-distance constraints versus long-distance constraints. For illustration purposes, in the examples which follow below, we shall always combine both short- and long-distance constraints. An important comment, however, is that when one uses only chiral constraints, the masses \tilde{M}_n appear to converge monotonously to the exact values, while if one also uses OPE constraints, this appears not to be true. Even so, the approximate Adler function, in all the numerical experiments we have examined, always gets better for all values of Q^2 if one includes more resonances in a systematic way.

We shall now construct explicitly the leading and next-to-leading Minimal Hadronic Approximation to the model.

3.1 ONE STATE PLUS CONTINUUM

The onset of the continuum is now

$$s_0 = \sigma^2, \quad (3.36)$$

and the first OPE constraint becomes

$$1 - 2 \frac{\tilde{M}_0^2}{\sigma^2} = -\frac{1}{12}. \quad (3.37)$$

The numerical value of the solution is

$$\tilde{M}_0^2 = 0.541667\sigma^2, \quad (3.38)$$

⁶Although not *necessarily* so. The Stieltjes function $\int_0^\infty dt \frac{e^{-t}}{1+zt}$, which has $\sum_{n=0}^\infty (-1)^n n! z^n$ as the asymptotic series for $z \rightarrow 0$, can actually be approximated in a convergent sequence of steps with this method [19].

not quite the exact value $M_0^2 = \frac{1}{2}\sigma^2$ of the *real spectrum* but not bad at all! In fact, as shown in Fig. 3, the simple MHA of one state plus continuum, already reproduces rather well the shape of the *exact* Adler function. For comparison, if \tilde{M}_0^2 is fixed using the first χ PT constraint, one finds $\tilde{M}_0^2 = 0.504125\sigma^2$. While this is much closer to the exact value $M_0^2 = 0.5\sigma^2$, the approximate Adler function turns out to be a worse approximation for $Q^2 \gtrsim 1.8\sigma^2$.

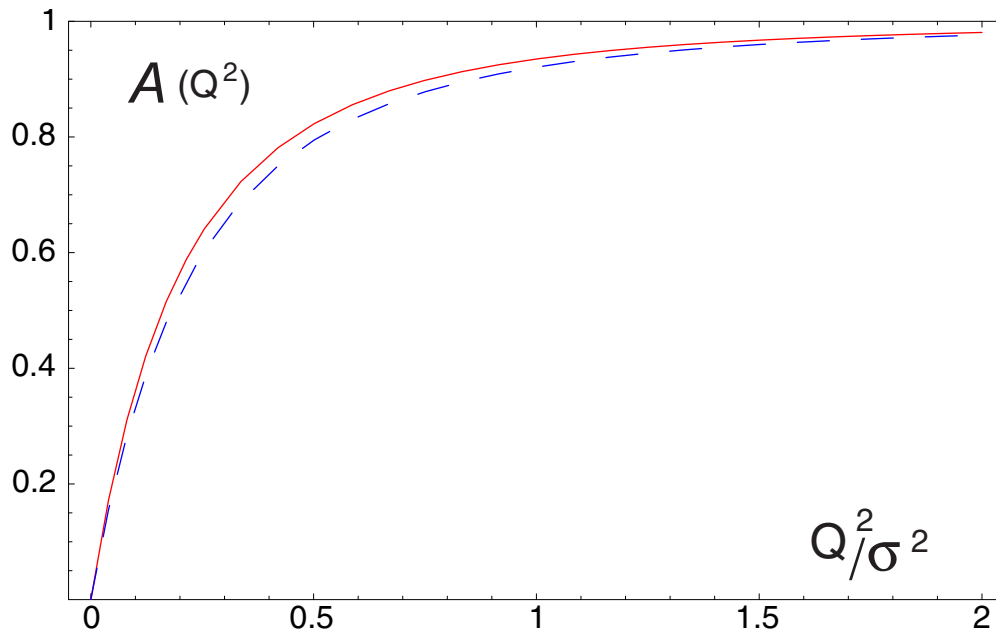


Fig. 3 The exact Adler function of the toy model (the continuous red curve), and the Adler function predicted by the MHA with one state plus continuum (the dashed blue curve), are plotted versus Q^2/σ^2 .

3.2 TWO STATES PLUS CONTINUUM

We can now tune the masses \tilde{M}_0 and \tilde{M}_1 to reproduce the leading $\frac{1}{Q^4}$ and next-to-leading $\frac{1}{Q^6}$ terms of the underlying OPE. The constraining equations are now

$$4 - 2\frac{\tilde{M}_0^2}{\sigma^2} - 2\frac{\tilde{M}_1^2}{\sigma^2} = \frac{-1}{12}, \quad (3.39)$$

$$-8 + 3\frac{\tilde{M}_0^4}{\sigma^4} + 3\frac{\tilde{M}_1^4}{\sigma^4} = 0. \quad (3.40)$$

They lead to the solutions:

$$\tilde{M}_0^2 = 0.481174\sigma^2 \quad \text{and} \quad \tilde{M}_1^2 = 1.56049\sigma^2, \quad (3.41)$$

instead of the physical values $M_0^2 = \frac{1}{2}\sigma^2$ and $M_1^2 = \frac{3}{2}\sigma^2$. Notice that the mass of the ground state in the two state approximation gets closer to the physical mass. The corresponding Adler function also approaches better the *exact* Adler function. In order to quantify this improvement we plot in Fig. 4

the difference of functions

$$\Delta^{(1)} \equiv \mathcal{A}(Q^2) - \mathcal{A}(Q^2) \Big|_{\text{MHA}}^{(1)} \quad \text{and} \quad \Delta^{(2)} \equiv \mathcal{A}(Q^2) - \mathcal{A}(Q^2) \Big|_{\text{MHA}}^{(2)}, \quad (3.42)$$

versus Q^2 .

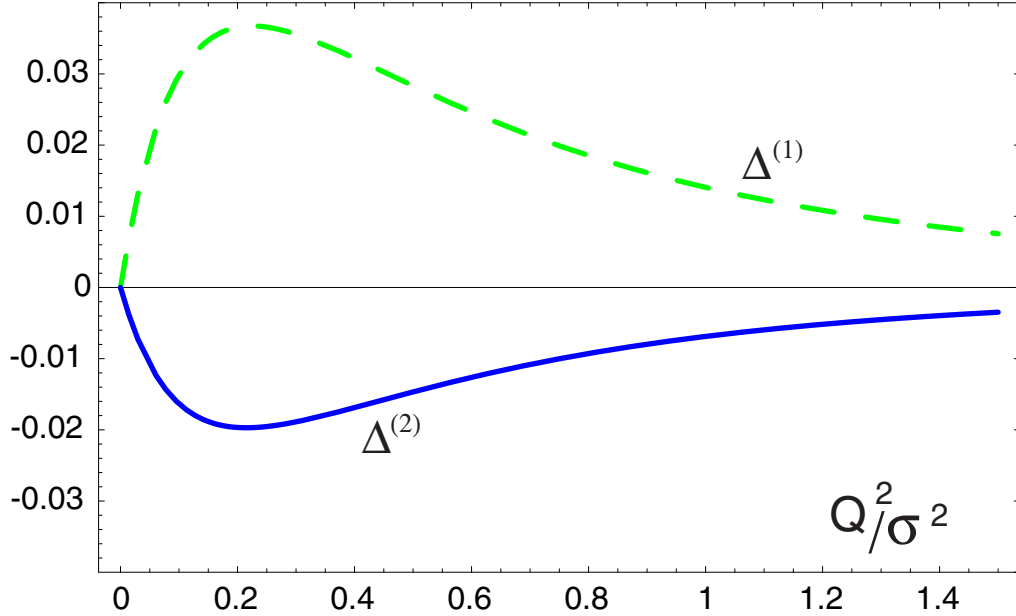


Fig. 4 The difference of Adler functions defined in Eq. (3.42) corresponding to the MHA with one state plus continuum (the dashed green curve) and with two states plus continuum (the continuous blue curve) are plotted versus Q^2/σ^2 . Notice the vertical scale in the plot.

Another alternative is to use as constraints the leading $\frac{1}{Q^4}$ behaviour of the OPE and the leading Q^2 behaviour of the chiral expansion. The constraining equations are then

$$4 - 2\frac{\tilde{M}_0^2}{\sigma^2} - 2\frac{\tilde{M}_1^2}{\sigma^2} = \frac{-1}{12}, \quad (3.43)$$

$$\frac{1}{2} + \frac{\sigma^4}{\tilde{M}_0^4} + \frac{\sigma^4}{\tilde{M}_1^4} = \frac{\pi^2}{2}; \quad (3.44)$$

and the corresponding numerical solutions for the masses are then:

$$\tilde{M}_0^2 = 0.499093\sigma^2 \quad \text{and} \quad \tilde{M}_1^2 = 1.54257\sigma^2. \quad (3.45)$$

They approach, even better, the *exact* masses than those previously obtained in Eq. (3.41). In fact, combining the leading short-distance constraint with the leading long-distance constraint turns out to produce an approximated Adler function much closer to the exact one. We illustrate this in Fig. 5 where the dashed blue curve is the same as the continuous blue curve in Fig. 4 (though plotted on a different scale), while the continuous red curve is the one obtained solving the constraints of Eq. (3.43). The improvement is rather remarkable. We would like to emphasize that in the applications of the MHA to large- N_c QCD that we have made so far in refs. [6] to [10], we have used equivalent constraints to the ones discussed in this example.

In Fig. 5 we use the following notation: $\Delta_{ij}^{(m)}$ indicates the difference between the exact Adler function and the one obtained using the MHA with m states plus continuum, with the masses obtained by solving a system of equations which consists of i short-distance constraints and j long distance constraints; i.e.,

$$\Delta_{ij}^{(m)} \equiv \mathcal{A}(Q^2) - \mathcal{A}(Q^2)|_{\text{MHA}}^{(m)} \left\{ \begin{array}{l} \text{with } i \text{ SD-constraints} \\ \text{and } j \text{ LD-constraints} \end{array} \right\}, \quad i + j = m. \quad (3.46)$$

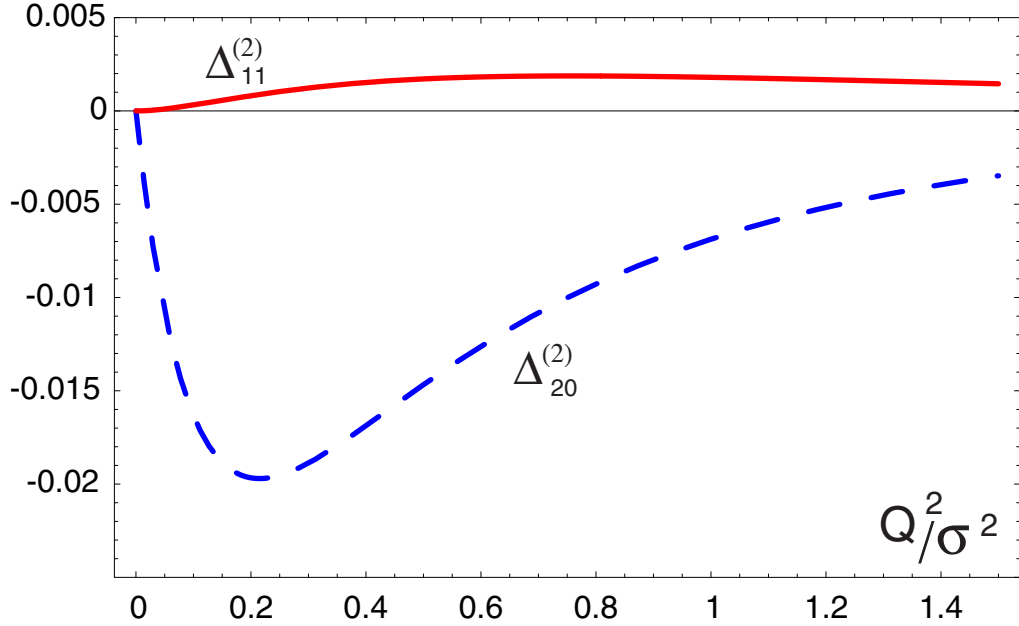


Fig. 5 The difference of Adler functions corresponding to the MHA with two states plus continuum. The dashed blue curve is the same as the one in Fig. 4, though on a different scale, while the continuous red curve is the one obtained using as input masses the solutions in Eq. (3.45).

We have constructed the MHA with up to 11 resonances. With a similar number of short-distance and long-distance constraints, the maximum difference between MHA and the exact Adler function is always decreasing by half an order of magnitude (in average) every time a new resonance is explicitly included in the MHA. This maximum difference occurs for Q^2 at roughly 1/3 of the number of resonances included. For instance for 11 resonances this maximum difference is of the order of 10^{-8} and happens at $Q^2/\sigma^2 \simeq 4$.

4 Finite-Energy Sum Rules and Hadronic Duality.

In every day life QCD, the paradigm of a finite-energy sum rule (FESR) is the one provided by the hadronic decay of the τ , which relates the branching ratio

$$\mathcal{R}_\tau = \frac{\Gamma(\tau^- \rightarrow \nu_\tau \text{ Hadrons})}{\Gamma(\tau^- \rightarrow \nu_\tau e^- \bar{\nu}_e)}, \quad (4.47)$$

to the vector and axial-vector hadronic spectral functions. In the chiral limit, this relation is simply given by the integral⁷

$$\mathcal{R}_\tau(s) = \int_0^s \frac{dt}{s} \left(1 - \frac{t}{s}\right)^2 \left(1 + 2\frac{t}{s}\right) \frac{1}{\pi} \text{Im}\Pi(t), \quad (4.48)$$

for $s = m_\tau^2$. Sum rules of this type have been extensively studied in the literature⁸ and proved very useful for extracting the value of the QCD running coupling constant. The toy model offers an interesting theoretical laboratory to check these sum rules. Some observations in this respect have already been made by Shifman [15]. For the sake of clarity, we reproduce part of his analysis in our discussion.

Equation (4.48) is a combination of moment sum rules of the type

$$\mathcal{M}^{(p)}(s) = \int_0^s \frac{dt}{s} \left(\frac{t}{s}\right)^p \frac{1}{\pi} \text{Im}\Pi(t). \quad (4.49)$$

In the toy model, with the input spectral function in Eq. (2.2), these moments can be explicitly calculated with the result

$$\mathcal{M}^{(p)}(s) = \sigma^2 \sum_{n=0}^{\frac{s}{\sigma^2} - \frac{1}{2} - x} \frac{(n + \frac{1}{2})^p \sigma^{2p}}{s^{p+1}}, \quad (4.50)$$

where $0 \leq x < 1$ is the fractional part of $\frac{s}{\sigma^2} - \frac{1}{2}$; in other words,

$$s = (m + x + \frac{1}{2})\sigma^2, \quad \text{for } m = 0, 1, 2, \dots \quad (4.51)$$

The exact $\mathcal{R}_\tau(s)$ in the toy model of large- N_c is then

$$\mathcal{R}_\tau(s) = \frac{1}{2} - \frac{1}{2} \left(\frac{\sigma^2}{s}\right)^3 x(1-x)(1-2x) + \frac{1}{2} \left(\frac{\sigma^2}{s}\right)^4 \left[x^2(1-x)^2 - \frac{1}{16} \right]. \quad (4.52)$$

This expression could be viewed as the *exact* $\mathcal{R}_\tau(s)$ calculated from the *data* in an imaginary world in which the τ mass may be dialed to be as large as one wishes. This exact $\mathcal{R}_\tau(s)$ is plotted in Fig. 6 versus the ratio s/σ^2 (the red continuous curve) and as it can be seen, it shows a damped oscillatory behaviour induced by the convolution in the integrand of $\mathcal{R}_\tau(s)$ in Eq. (4.48) of a decreasing polynomial in s and an infinite set of equally-spaced “kicks” (i.e. the narrow resonances). Should the number of resonances stop at a certain finite number m , beyond which the continuum takes over, the oscillations for $\frac{s}{\sigma^2} > m + \frac{1}{2}$ would disappear and turn into an ordinary power fall-off towards the value of the parton model, i.e. $1/2$.

It is interesting to compare the exact $\mathcal{R}_\tau(s)$ function in Eq. (4.52) with the one predicted by the OPE of the same model. Emulating what is being done in the real-world analysis of τ decay, this comparison can be obtained from an integral representation in the complex z -plane (where $z = Q^2/s$),

$$\mathcal{R}_\tau(s) = \frac{-1}{2\pi i} \oint_{|z|=1} dz (1+z)^2 (1-2z) \Pi(zs) \quad (4.53)$$

$$= \frac{1}{2\pi i} \oint_{|z|=1} \frac{dz}{z} \left(\frac{1}{2} - z + z^3 + \frac{1}{2} z^4 \right) \mathcal{A}(zs), \quad (4.54)$$

by inserting the OPE for the Adler function in Eq. (2.14). Doing this one notices that, besides the partonic contribution, only the powers proportional to $1/Q^2$, $1/Q^6$ and $1/Q^8$ in the OPE of the Adler function contribute to the integral, with the result

⁷Here we only consider the vector, and not the axial-vector, part.

⁸See e.g. refs. [20, 21].

$$\mathcal{R}_\tau^{\text{OPE}}(s) = \frac{1}{2} - \frac{7}{480} \left(\frac{\sigma^2}{s} \right)^4 \quad (4.55)$$

The curve corresponding to this $\mathcal{R}_\tau^{\text{OPE}}(s)$ function is also plotted in Fig. 6 (the blue dashed curve). It interpolates rather well the *exact* curve but it fails to reproduce its oscillations [15]. This is another manifestation of the violation of local duality (i.e. point-wise; as opposed to global duality, i.e. on average) between the quark–gluon picture represented by the OPE and the hadron picture represented by the full spectrum–based solution.

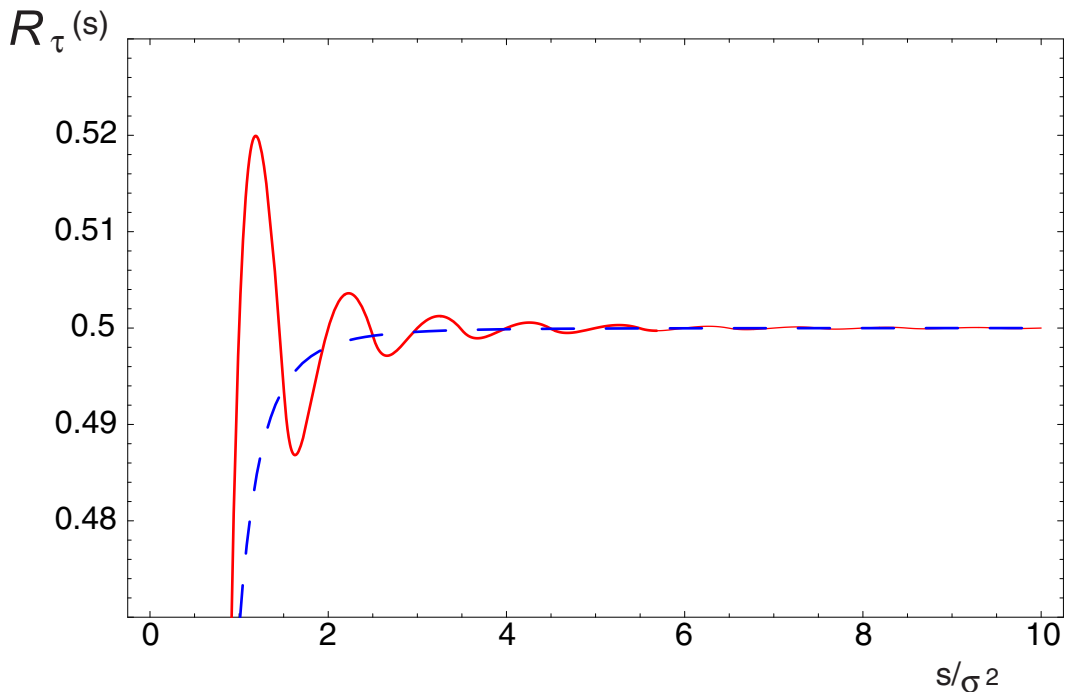


Fig. 6 Plot of the branching ratio $\mathcal{R}_\tau(s)$ defined in Eq. (4.48). The continuous red curve is the one predicted by the exact toy model; the dashed blue curve is the one predicted using the OPE.

However, one should also notice in this figure that there are “optimal” points at $s/\sigma^2 \approx m/2$, $m = 2, 3, 4, \dots$ where the difference between the oscillation and the OPE curve nearly vanishes. These “optimal” points are very useful because they allow the OPE to produce a very accurate result even at very low values of s/σ^2 ! We shall now elaborate on these special points and explain where they come from. To this end it is useful to identify clearly from \mathcal{R}_τ the combination which goes into $\mathcal{R}_\tau^{\text{OPE}}$ and the one which goes into $\mathcal{R}_\tau^{\text{OSC}}$. This can be readily obtained by rewriting $\mathcal{R}_\tau(s)$ in Eq. (4.52) as a linear combination of Bernoulli polynomials in the x variable. Using Eqs. (A.8) and (A.9) we can rewrite

$$\mathcal{R}_\tau(s) = \mathcal{R}_\tau^{\text{OPE}}(s) + \mathcal{R}_\tau^{\text{OSC}}(s), \quad (4.56)$$

with $\mathcal{R}_\tau^{\text{OPE}}(s)$ as given in Eq. (4.55), and

$$\mathcal{R}_\tau^{\text{OSC}}(s) = - \left(\frac{\sigma^2}{s} \right)^3 B_3(x) + \frac{1}{2} \left(\frac{\sigma^2}{s} \right)^4 B_4(x). \quad (4.57)$$

The oscillatory nature of this expression follows from the Fourier decomposition of the Bernoulli polynomials, as given in Eqs. (A.15) and (A.16), with the result

$$\mathcal{R}_\tau^{\text{OSC}}(s) = -12 \sum_{n=1}^{\infty} \left\{ \left(\frac{\sigma^2}{s} \right)^3 \frac{\sin \left[2\pi n \left(\frac{s}{\sigma^2} - \frac{1}{2} \right) \right]}{(2\pi n)^3} + 2 \left(\frac{\sigma^2}{s} \right)^4 \frac{\cos \left[2\pi n \left(\frac{s}{\sigma^2} - \frac{1}{2} \right) \right]}{(2\pi n)^4} \right\}, \quad (4.58)$$

where we have used the fact that x , defined in Eq. (4.51), is equivalent to $\frac{s}{\sigma^2} - \frac{1}{2}$ in the argument of $\sin [2\pi nx]$ and/or $\cos [2\pi nx]$. Equation (4.58) shows the oscillations decomposed in terms of harmonics. Interestingly, one sees that the leading oscillation at large s , i.e. $\sim 1/s^3$, cancels exactly for values of s/σ^2 which are integers or half-integers, i.e. $\frac{s}{\sigma^2} = \frac{k}{2}$, $k = 0, 1, 2, \dots$ ⁹ The set of half-integers coincide with the exact location of the resonances and would correspond in the case of true QCD to the masses in the large- N_c limit, which is information one does not have in real life. However, the integer values coincide with the condition on s in Eq. (3.33), namely $s = (m+1)\sigma^2$. This is more useful since it only relies on the matching of the MHA onto the first term of the OPE which is always available. Of course, it is not known to what extent a similar relation there exists between the leading oscillatory term and the $1/Q^2$ term in the OPE for the case of large- N_c QCD; these features may very well be generic, and should be kept in mind when dealing with phenomenological studies of finite-energy sum rules in QCD. Indeed, the analysis of Ref. [22] shows that the data seem to support this.

The representation in Eq. (4.58) neatly disentangles the effect of the spectrum (the infinite sum over the oscillatory terms) from its projection on the particular observable we are considering; in this case \mathcal{R}_τ , which is only sensitive to the two powers $(\sigma^2/s)^3$ and $(\sigma^2/s)^4$.

Looking at Fig. 6 makes it clear that an analysis of the data at a given value of s based solely on the OPE curve induces an error which is proportional to the size of the nearby oscillation. Consequently it is highly desirable to develop an approximation scheme which, at least in principle, can reproduce these oscillations. We shall now see that the MHA is such a scheme.

One example of the prediction from the MHA for \mathcal{R}_τ can be seen in Fig. 7. This example is the case of four resonances which are matched onto the first two long-distance and the first two short-distance constraints. Since the MHA has been constructed by matching on to the first few terms of the OPE, it has to reproduce the corresponding prediction of the OPE for \mathcal{R}_τ as soon as $s > s_0$, s_0 being the onset of the continuum of the MHA. Since \mathcal{R}_τ can only read the inverse powers up to and including $1/Q^8$, this means the MHA will reproduce the result of $\mathcal{R}_\tau^{\text{OPE}}$ provided at least three resonance masses are matched on to the corresponding three short-distance constraints corresponding to the powers $1/Q^4, 1/Q^6, 1/Q^8$ of the OPE (recall that the $1/Q^2$ power is always used to determine s_0). Since in the MHA curve in Fig. 7 only the first two inverse powers of Q^2 have been used, this explains the small difference between the MHA and the OPE curves in Fig. 7 at $s = s_0 = 4\sigma^2$. One can check that this difference disappears when the three short-distance constraints coming from the $1/Q^4, 1/Q^6, 1/Q^8$ powers of the OPE are used. This is not surprising. It is also not surprising that the MHA fits so well the low-energy region in Fig. 7, since the MHA has been matched onto the first two chiral powers at low energies. What is more interesting is how well the MHA also describes the intermediate region of s with all the oscillations. This result clearly goes beyond the input.

⁹Notice that for the value $x = 1/2$, the parton model and the exact result in Eq. (4.52) agree with each other. However, this is no longer true when $\hat{M}_0^2 \neq 1/2$. See also footnote 5.

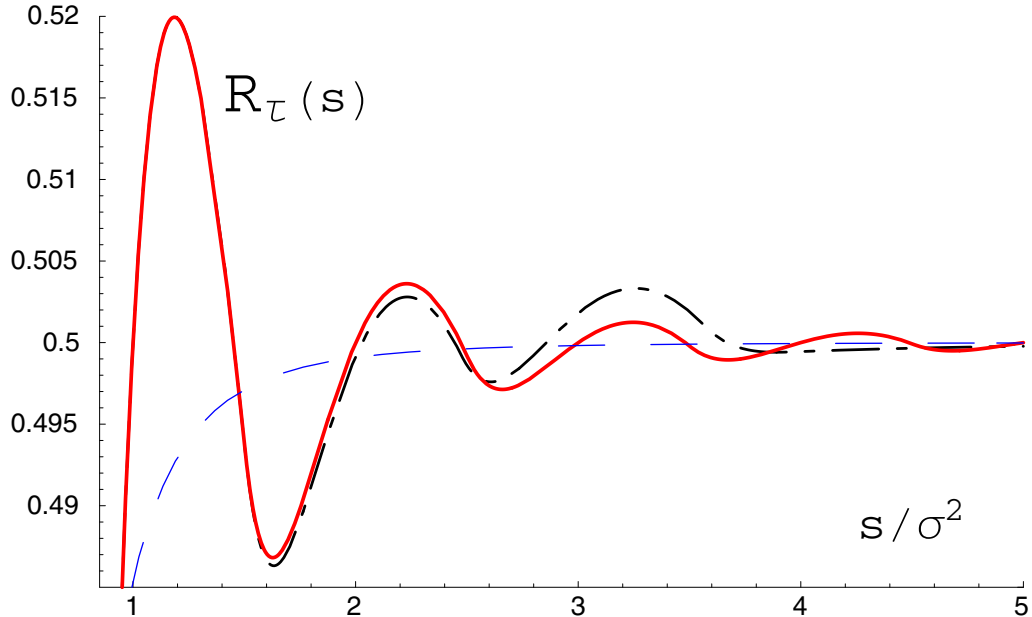


Fig. 7 Plot of the branching ratio $\mathcal{R}_\tau(s)$ defined in Eq. (4.48). As in Fig. 5, the continuous red curve is the exact result predicted by the toy model, the dashed blue curve is the one predicted using the OPE. The black dot-dashed curve is the prediction of the MHA. This curve has been produced with four resonances fixed by the first two short-distance and the first two long-distance constraints.

A useful conclusion, for phenomenological purposes, which emerges from these toy-model exercises is that, when confronting the real situation of a finite-energy sum rule involving *hadronic data* to QCD, say a sum rule of the type

$$\int_0^{s_0} dt \rho(t)_{\text{hadronic}} = F_{\text{QCD}}(s_0), \quad (4.59)$$

the s_0 values at which the comparison between theory and data should be made are not *arbitrary* [22], as is unfortunately often assumed in the literature; optimally, they must be made at the specific *duality* values which are appropriate solutions of the leading OPE constraints relevant to the case one is considering. Alternatively, one can choose the highest value of s available by the data (which in the real world is fixed by the τ mass) so as to minimize the size of the oscillations, and then use the MHA to approximate their shape. It would be very interesting to reanalyze τ data in these two new ways. The case of QCD is of course more complicated than that of our toy model, but our discussion of the toy model nevertheless suggests that both ways of analyzing real data should prove useful, and possibly lead to an estimate of the errors involved. In addition, one can extend the use of the toy model to investigate the MHA for other quantities of interest. Finally, we recall that a slightly more sophisticated version of the model does remarkably well phenomenologically [14], indicating that it does have something to do with the real solution of large- N_c QCD.

5 Acknowledgements

E. de R. and S. P. would like to thank the organizers of the workshop “Lattice QCD and Hadron Phenomenology” held at the INT, University of Washington at Seattle, where this work was finalized, for their kind invitation and warm hospitality. S.P. would also like to thank J. Carmona and E. Elizalde for discussions. M.G. thanks the IFAE at the Universitat Autònoma de Barcelona for hospitality.

The work of E. de R. and S.P. is supported by TMR, EC-Contract No. ERBFMRX-CT980169 (EURODA ϕ NE). The work of S.P. is also supported by CICYT-AEN99-0766, and that of M.G. in

part by the US Dept. of Energy.

A APPENDIX

1. Bernoulli Polynomial

The Bernoulli polynomials are defined as:

$$B_n(x) = \sum_{r=0}^n \binom{n}{r} B_r x^{n-r}, \quad (\text{A.1})$$

where

$$\binom{n}{r} = \frac{\Gamma(n+1)}{\Gamma(r+1)\Gamma(n-r+1)}, \quad (\text{A.2})$$

and B_{2n} are the Bernoulli numbers :

$$B_0 = 1, \quad B_1 = -\frac{1}{2}, \quad B_2 = \frac{1}{6}, \quad B_4 = -\frac{1}{30}, \quad B_6 = \frac{1}{42}, \quad \dots; \quad (\text{A.3})$$

with

$$B_{2n+1} = 0, \quad \text{for } n \geq 1. \quad (\text{A.4})$$

Examples of the first few Bernoulli polynomial are:

$$B_0(x) = 1, \quad (\text{A.5})$$

$$B_1(x) = x - \frac{1}{2}, \quad (\text{A.6})$$

$$B_2(x) = x^2 - x + \frac{1}{6}, \quad (\text{A.7})$$

$$B_3(x) = x^3 - \frac{3}{2}x^2 + \frac{1}{2}x, \quad (\text{A.8})$$

$$B_4(x) = x^4 - 2x^3 + x^2 - \frac{1}{30}. \quad (\text{A.9})$$

The Bernoulli numbers are related to the Riemann zeta function of even argument:

$$B_{2n} = (-1)^{n+1} (2\pi)^{-2n} 2(2n)! \zeta(2n), \quad \text{for } n = 0, 1, 2, \dots \quad (\text{A.10})$$

Other important relations for Bernoulli polynomials are:

$$B_n(x=0) = B_n, \quad (\text{A.11})$$

$$B_n(x+1) - B_n(x) = nx^{n-1}, \quad (\text{A.12})$$

$$B_n(1-x) = (-1)^n B_n(x), \quad (\text{A.13})$$

$$B'_n(x) = nB_{n-1}(x). \quad (\text{A.14})$$

It is sometimes useful to recall the trigonometric expansion of Bernoulli polynomials, for $N \geq 1$:

$$B_{2N}(x) = (-1)^{N+1} 2(2N)! \frac{1}{(2\pi)^{2N}} \sum_{n=1}^{\infty} \frac{\cos 2\pi n x}{n^{2N}}, \quad (\text{A.15})$$

$$B_{2N+1}(x) = (-1)^{N+1} 2(2N+1)! \frac{1}{(2\pi)^{2N+1}} \sum_{n=1}^{\infty} \frac{\sin 2\pi n x}{n^{2N+1}}. \quad (\text{A.16})$$

References

- [1] G. 't Hooft, Nucl. Phys. **B72** (1974) 461; **B73** (1974) 461.
- [2] *The large N Expansion in Quantum Field Theory and Statistical Physics*, Editors E. Brézin and S.R. Wadia, World Scientific, 1993.
- [3] A.V. Manohar, *Large- N_c QCD*, in les Houches Session LXVIII, North Holland, 1999.
- [4] S. Coleman and E. Witten, Phys. Rev. Lett. **45** (1980) 100.
- [5] E. Witten, Nucl. Phys. **B160** (1979) 57.
- [6] M. Knecht, S. Peris and E. de Rafael, Phys. Lett. **B443** (1998) 255.
- [7] M. Knecht, S. Peris, M. Perrottet and E. de Rafael, Phys. Rev. Lett. **83** (1999) 5230.
- [8] S. Peris and E. de Rafael, Phys. Lett. **B490** (2000) 213, *erratum* hep-ph/0006146 v3.
- [9] M. Golterman and S. Peris, Phys. Rev. **D61** (2000) 034018.
- [10] M. Knecht, S. Peris and E. de Rafael, Phys. Lett. **B508** (2001) 117.
- [11] C.G. Callan Jr., N. Coote and D.J. Gross, Phys. Rev. **D13** (1976) 1649; M.B. Einhorn, Phys. Rev. **D14** (1976) 3451.
- [12] A. Bramon, E. Etim and M. Greco, Phys. Lett. **B 41** (1972) 609; M. Greco, Nucl. Phys. **B 63** (1973) 398. J.J. Sakurai, Phys. Lett. **B46** (1973) 207. For its connection to Regge Theory, see G. Veneziano, Nuovo Cim. **A 57** (1968) 190.
- [13] B.V. Geshkenbein, Sov. J. Nucl. Phys. **49** (1989) 705.
- [14] M. Golterman and S. Peris, JHEP01 (2001) 028.
- [15] M. Shifman, *Quark-Hadron Duality*, hep-ph/0009131.
- [16] E.T. Whittaker and G.N. Watson, *A Course of Modern Analysis*, Ch. XIII, 4th ed., Cambridge University Press, 1965.
- [17] M.A. Shifman, A.I. Vainshtein and V.I. Zakharov, Nucl. Phys. **B147** (1979) 385, *ibid* 447.
- [18] E. de Rafael, *Large- N_c QCD and Low Energy Interactions*, hep-ph/0110195.
- [19] C.M. Bender and S. A. Orszag, “Advanced Mathematical Methods for Scientists and Engineers. Asymptotic Methods and Perturbation Theory”, McCraw-Hill, 1978. Example 6 in section 8.5.
- [20] E. Braaten, S. Narison and A. Pich, Nucl. Phys. **B373** (1992) 581.
- [21] F. Le Diberder and A. Pich, Phys. Lett. **B289** (1992) 165.
- [22] S. Peris, B. Phily and E. de Rafael, Phys. Rev. Lett. **86** (2001) 14; S. Peris, M. Perrottet and E. de Rafael, JHEP05 (1998) 011.